

## **PROGRESS TOWARD BROAD-BAND AMBIENT NOISE TOMOGRAPHY IN EURASIA**

Michael H. Ritzwoller<sup>1</sup>, Michael Pasyanos<sup>2</sup>, Yingjie Yang<sup>1</sup>, Anatoli L. Levshin<sup>1</sup>, Nikolai M. Shapiro<sup>1</sup>  
University of Colorado at Boulder<sup>1</sup>, Lawrence Livermore National Laboratory<sup>2</sup>

Sponsored by National Nuclear Security Administration  
Office of Nonproliferation Research and Development  
Office of Defense Nuclear Nonproliferation

Contract No. DE-FC52-2005NA26607 and W-7406-ENG-48

### **ABSTRACT**

We extend ambient noise surface wave tomography both in band-width (6 sec - 50 sec period) and geographical extent (across much of Europe) compared with previous applications. The data are taken from about 125 broad-band seismic stations from the Global Seismic Network (GSN) and the Orfeus Virtual European Broad-band seismic Network (VEBSN). Cross-correlations are computed in daily segments, stacked over one-year (2004), and Rayleigh wave group dispersion curves from 6 sec – 50 sec period are measured using a phase-matched filter, frequency-time analysis technique. We estimate measurement uncertainties using the seasonal variation of the dispersion curves revealed in three-month time series. On average, uncertainties in group delays increase with period from ~3 sec to ~7 sec from periods of 10 sec - 50 sec, respectively. Group speed maps at periods from 8 sec to 40 sec are estimated, and the resulting path coverage is denser and displays a more uniform azimuthal distribution than from earthquake-emitted surface waves. The fit of the group speed maps to the ambient noise data is significantly improved below 30 sec compared to the fit achieved with earthquake data. Average resolution is estimated to be about 100 km at 10 sec period, but degrades with increasing period and toward the periphery of the study region. The resulting ambient noise group speed maps demonstrate significant agreement with known geologic and tectonic features. In particular, the signatures of sedimentary basins and crustal thickness are revealed clearly in the maps. These results are evidence that surface wave tomography based on cross-correlations of long time-series of ambient noise data can be achieved over a broad period band on nearly a continental scale and yield higher resolution and more reliable group speed maps than based on traditional earthquake-based measurements. Final application of the method in Europe would benefit from processing a second year of data in order to increase the signal-to-noise level, improve the uncertainty estimates, and increase the size of the dataset. Application of ambient noise tomography to other areas with dense station coverage in Eurasia is a natural extension of this work.

## **OBJECTIVE**

The goal of this research is to develop the new method to obtain surface wave dispersion measurements based on ambient seismic noise and to produce a new dataset of interstation group velocity measurements. These new data are used to produce improved group velocity tomographic maps, particularly at short periods (< 20 sec).

## **RESEARCH ACCOMPLISHED**

### **Introduction**

Traditional inference of seismic wave speeds in Earth's interior is based on observations of waves emitted by earthquakes or human-made explosions. Surface wave tomography has proven particularly useful in imaging Earth's crust and uppermost mantle on both regional and global scales. Because they propagate in a region directly beneath Earth's surface, surface waves typically generate better path coverage of the upper regions of Earth than body waves with the same distribution of seismic stations. There are, however, basic limitations to earthquake-based surface wave tomography independent of the number of broad-band stations available. First, due to the uneven distribution of earthquakes around the world, seismic surface waves only sample certain preferential azimuths. In addition, in aseismic regions surface wave dispersion can be measured only from distant earthquakes. Second, it is difficult to obtain high-quality short-period (<20 sec) dispersion measurements from teleseismic events due to intrinsic attenuation and scattering along ray paths. It is, however, the short-period waves that are most useful to constrain the structure of the crust and uppermost mantle. Third, inversions of seismic surface waves require some information about sources, such as earthquake hypocentral locations and moment tensors in some cases, which have a substantial intrinsic inaccuracy, particularly for small events. Some of the problems that beset traditional earthquake surface wave tomography can be alleviated by observations made on diffuse wavefields (e.g., ambient noise, scattered coda waves). Theoretical research has shown that, under the right circumstances, the time-derivative of the cross-correlation of records of ambient noise from two seismic stations provides an estimate of the Green function between the stations, modulated by the spectrum of the noise source (Weaver and Lobkis, 2001, 2004; Derode et al., 2003; Snieder, 2004). Ambient noise tomography has been applied successfully at very short periods over small regions (e.g. in S. California, Shapiro et al., 2005, Sabra et al., 2005; in S. Korea, Cho et al., 2006). The purpose of this research is to determine whether ambient noise Rayleigh wave tomography can be applied reliably on a nearly continental scale and extended from short (~6 sec) to intermediate periods (~ 50 sec). More details about this method are given by Yang et al. (2006). Final application of the method in Eurasia would benefit from adding a second year data, to improve the signal level, improve uncertainty estimate,

### **Data processing and group velocity measurements**

Europe is an excellent region to test ambient noise surface wave tomography. Broad-band seismic station coverage is dense across much of the continent and the substantial a priori knowledge of geological structures allows us to evaluate the reliability of the resulting group velocity maps. We have collected continuous vertical-component seismic data from 125 stations including data from the Global Seismic Network (GSN) and the Virtual European Broad-Band Seismic Network (VEBSN) (Figure 1) over the 12 months of 2004. About 110 of these stations returned useful data.

The data processing procedure that is applied here is very similar to that discussed at greater length in the paper by Bensen et al. (2006). The data processing method was evolved significantly since the first work by Shapiro et al. (2005). Using vertical-component seismic data implies that the resulting cross-correlations contain only Rayleigh wave signals. Data are processed one day at a time for each station after being decimated to 1 sample per second and are band-pass filtered in the period band from 5 to 150 sec after the daily trend, the mean and the instrument response are removed. Data are then normalized in time and whitened over the frequency-band of interest prior to cross-correlation.

After the time-series has been processed for each day, we then compute daily cross-correlations in the period band from 5 to 150 sec and then stack the results into a set of three-month and one-year time series. The three-month stacks are used to investigate the seasonal variability of the measurements, which is the basis for the error analysis and is part of the data selection procedure discussed further below. An example of a broad-band (5 to 150 sec) symmetric-component cross-correlation for the station pair IBBN and TIRR is shown in Figure 2 together with the

cross-correlation filtered into five frequency sub-bands. Rayleigh waves emerge clearly in each frequency band with the earlier arriving waves being at longer periods.

To begin to evaluate the quality of the cross-correlations quantitatively, we calculate the signal-to-noise ratio (SNR) for each cross-correlation. SNR is defined as the ratio of the peak amplitude within a time window containing the signals to the root-mean-square of noise trailing the signal arrival window. Because the SNR can vary strongly with frequency, we filter the broad-band cross-correlations into three narrower pass-bands at 8-25 sec, 20-50 sec and 33-70 sec and compute the SNR in each band. We reject cross-correlations with SNR less than 7 in each band. Group velocity curves are measured on the estimated Green functions that emerge from both the three-month and one-year stacks in each of the three period bands using automatic Frequency Time Analysis (FTAN) as described by Bensen et al. (2006) in detail.

### **Data selection and uncertainty estimation**

The automated measurement procedure must be followed by the application of criteria to select the data. We apply three general types of criteria: (1) signal-to-noise ratio (SNR), (2) repeatability of the measurements (particularly seasonal variability), and (3) coherence across the set of measurements. The formal uncertainty analysis is based on seasonal variability.

First, we reject a cross-correlation if its  $SNR < 7$ . Figure 3a shows an example histogram of the distribution of SNR for signals band-pass filtered between 20 and 50 sec. Distributions are similar in the other two pass-bands, between 8 and 25 sec and between 33 and 70 sec.

Second, for a measurement to be accepted, it needs to be repeatable in the sense that measurements obtained at different times should be similar. The repeatability criterion is based on quantifying seasonal variability. To do so, we select 12 over-lapping three-month time-series for each station-pair. Figure 4 shows an example of the seasonal variability in the observed dispersion curves. The dispersion curves that are used for tomography here are taken from the 12-month stacks. The standard deviation is computed for a station-pair if more than 4 three-month stacks have a  $SNR > 7$ . The measurement is retained if the standard deviation is less than 100 m/sec. It is rejected if the standard deviation either cannot be computed due to the fact that too few measurements can be obtained on the 3-month stacks or if the standard deviation is too large. The effect of this step in eliminating measurements is shown in Figure 3b. Figures 3d and 3e show the average measurement uncertainties taken over the entire European data set. Average uncertainties of group velocities and group arrival times increase with period from  $\sim 0.02$  km/s or  $\sim 3$  sec at 10 sec period to 0.09 km/s or 7.5 sec at 50 sec period.

Third, we require that the measurements cohere with one another across the data set. Incoherent measurements that disagree with other measurements in the data set are identified during tomography.

Finally, we find that to obtain a reliable measurement, the stations must be separated by at least 3 wavelengths.

The number of measurements that remain after all criteria have been applied is shown in Figure 3b. Less than a third of the original measurements are retained for tomography. The least satisfying part of the procedure is eliminating what appears to be a good measurement on the 12-month stack because the uncertainty estimate could not be determined, usually because of an insufficient number of high SNR 3-month stacks. To retain a higher percentage of measurements, it will be necessary to process two or more years of data. This would increase the SNRs of the seasonal stacks and be preferable over a single year of data. Bensen et al. (2006) discuss this further.

### **Surface wave tomography**

The dispersion measurements of Rayleigh waves from one-year cross-correlations are used to invert for group velocity maps on a  $1^\circ \times 1^\circ$  grid across Europe using the tomographic method of Barmin et al. (2001). Uncertainty estimates exist for every measurement, and have been used as weights in the inversion. Resolution is estimated using the method described by Barmin et al. (2001) with modifications presented by Levshin et al. (2005).

Group speed tomography is performed in two steps. The first, preliminary, step generates overly smoothed maps at each period in order to identify and reject any remaining bad measurements. The over-smoothed model is able to fit most data fairly well. We discard group velocity measurements with travel time residuals larger than 15 sec, which is about the RMS value of the travel time residuals at most periods. The number of paths remaining after this step of data reduction is shown in Figure 3b.

The second step of tomography is the construction of the final maps. Maps are defined relative to the reference maps computed from the 3-D model of Shapiro and Ritzwoller (2002). In an important sense, the reference maps already have a priori information imposed on crustal structure. The 3-D model itself was constructed as a perturbation to a starting model that included information about sediments and crustal thicknesses. For this reason, we choose to seek only smooth perturbations to the reference maps.

Examples of path density and resolution are shown in Figure 5 for the 16 sec measurements. Results are similar from 10 sec to 50 sec period. Path density is highest in the center of Europe and gradually degrades toward the edge of the study region. Average resolution is estimated to be about 100 km in the center of the study region in Europe, and like path density degrades toward the periphery of the map where station coverage is minimal.

The results of group velocity tomography at 10, 16, 20, 30, and 40 sec periods are shown in Figures 6 and 7a. Figures 7b illustrates that the perturbations to the reference model introduced during tomography are smooth and occur only in regions where path coverage is high, predominantly in the center of the region of study. In most of the Mediterranean Sea, the Atlantic Ocean, North Africa, the Iberian Peninsula, and far eastern Europe, the perturbations are small and the estimated maps are very similar to the reference maps. Many of the observed anomalies are correlated with known geological units, which is discussed further in the following paragraphs.

At the short-period end of this study (8-20 sec), group velocities are dominantly sensitive to shear velocities in the upper crust. Because the seismic velocities of sediments are very low, short-period low velocity anomalies are a good indicator of sedimentary basins. At the intermediate periods of this study (25-40 sec), Rayleigh waves are primarily sensitive to crustal thickness and the shear velocities in the lower crust and uppermost mantle. To aid assessment, Figure 6e and 6f presents a map of sediment thickness from CRUST1.0, which Laske and Masters digitized across most of Europe from the EXXON Tectonic Map of the World (Laske and Masters, 1997), and a map of crustal thickness taken from CRUST2.0 (Bassin, et al., 2000). We identify the names of several geological units on these maps, mainly sedimentary basins and mountain ranges.

The 10 sec and 16 sec group speed maps in Figures 6 and 7 exhibit low velocity anomalies associated with most of the known sedimentary basins across Europe. In regions of high data coverage, low-velocity anomalies are observed in the North Sea Basin, the Silesian Basin (North Germany, Poland), the Pannonian Basin (Hungary, Slovakia), the Po Basin (North Italy), the Rhone Basin (Southern France), and the Adriatic Sea. At intermediate periods (25 to 40 sec), the estimated maps exhibit low-velocity anomalies associated with the Alps, the Carpathians and the mountains in the Balkan region. The low velocity anomalies are probably caused by deeper crustal roots beneath mountain regions which occur due to isostatic compensation. The general reduction in Rayleigh wave velocity in the eastern part of the 30 - 40 sec maps in Figures 6 is probably related to the general thickening of the crust toward the east European craton.

Figure 8a shows the improvement in fit to the measured dispersion curves achieved by the resulting group velocity maps, expressed as the variance reduction relative to the predicted group velocity maps. In addition, variance reduction relative to the average across each map is shown. Variance reductions relative to predicted group velocity (solid line) are larger at short periods (< 25 sec) and smaller at long periods (>35 sec) than relative to the average (dashed line). Variance reductions are highest at short periods and gradually decrease with period. The observed trend of variance reductions is caused by group speed anomalies being largest at short periods and also because the 3-D model is more reliable for the longer periods. The RMS group velocity and travel time misfits after tomography are also shown in Figures 8b and 8c. Travel time misfit of the final data set is ~5 - 6 sec and is nearly independent of period.

## **CONCLUSIONS**

In this study, we use ambient noise data recorded at 125 broad-band seismic stations available from the Global Seismic Network (GSN) and the Orfeus Virtual European Broad-band seismic Network (VEBSN). All dispersion measurements have uncertainty estimates that derive from observations of seasonal variability. The data set would benefit from time-series of 2 or more years, which would allow more uncertainties to be measured and, therefore, more measurements will pass the selection criterion.

Group velocity maps at periods from 8 sec to 50 sec are obtained using ambient noise tomography. These maps provide a significant improvement in the understanding of surface wave dispersion in Europe, particularly at periods below about 20 sec. This study has denser and more uniform data coverage and demonstrates higher resolution than previous studies, which have relied on traditional earthquake-based surface wave tomography. The group velocity maps agree well with known geologic features, such as sedimentary basins and the lateral variation of crustal thickness. Observations at short periods (8 - 20 sec) provide entirely new constraints on sediment thickness, crustal thickness, and the shear velocity structure of crust.

In summary, this study demonstrates that surface wave tomography based on cross-correlations of long time-series of ambient noise data can be achieved over a broad period band on a nearly continental scale and yield higher resolution and more reliable group velocity maps than based on traditional earthquake-based measurements.

## **ACKNOWLEDGMENTS**

All of the data used in this research were downloaded from the continuous ftp database of the Orfeus

(Observatories and Research Facilities for European Seismology) Data Center and from the IRIS Data Management Center. In particular, the authors are deeply grateful to the data contributors to the Virtual European Broadband Seismic Network (VEBSN), a partnership of more than 30 local, regional and global arrays and network. The list of contributors is located at <http://www.orfeus-eu.org/meridian/vebsn-contributors.htm>. This research was supported by a contract from the US Department of Energy, DE-FC52-2005NA26607.

## **REFERENCES**

- Barmin, M.P., M.H. Ritzwoller, and A.L. Levshin (2001). A fast and reliable method for surface wave tomography, *Pure Appl. Geophys.*, **158**, 1351 - 1375.
- Bassin, C., Laske, G. and Masters, G. (2000). The current limits of resolution for surface wave tomography in North America, *EOS Trans AGU*, **81**, F897.
- Bensen, G.D., M.P. Barmin, F.-C. Lin, M.P. Moschetti, Y. Yang, A.L. Levshin, N.M. Shapiro, and M.H. Ritzwoller (2006). Obtaining robust group and phase speed curves for ambient noise tomography, manuscript in preparation.
- Cho, K.H., R.B. Hermann, C.J. Ammon, and K. Lee (2006). Imaging the upper crust of the Korean Peninsula by surface-wave tomography, *Bull. Seism. Soc. Amer.*, submitted.
- Derode, A., E. Larose, M. Tanter, J. de Rosny, A. Tourim, M. Campillo, and M. Fink (2003). Recovering the Green's function from field-field correlations in an open scattering medium (L), *J. Acoust. Soc. Am.*, **113**, 2973-2976.
- Laske, G. and G. Masters (1997). A Global Digital Map of Sediment Thickness, *EOS Trans. AGU*, **78**, F483.
- Levshin, A.L., M.P. Barmin, M.H. Ritzwoller, and J. Trampert (2005). Minor-arc and major-arc global surface wave diffraction tomography, *Phys. Earth Planet. Ints.*, **149**, 205-223.
- Sabra, K. G., P. Gerstoft, P. Roux, W. A. Kuperman, and M. C. Fehler (2005). Surface wave tomography from microseism in southern California, *Geophys. Res. Lett.*, **32**, L14311, doi:10.1029/2005GL023155.
- Shapiro, N.M. and M.H. Ritzwoller (2002). Monte-Carlo inversion for a global shear velocity model of the crust and upper mantle, *Geophys. J. Int.*, **151**, 88-105.
- Shapiro, N.M. M. Campillo, L. Stehly, and M.H. Ritzwoller (2005). High resolution surface wave tomography from ambient seismic noise, *Science*, **307**, 1615-1618.
- Snieder, R. (2004). Extracting the Green's function from the correlation of coda waves: A derivation based on stationary phase, *Phys. rev. E*, **69**, 046610.
- Weaver, R.L. and O.I. Lobkis, (2001). On the emergence of the Green's function in the correlations of a diffuse field, *J. Acoust. Soc. Am.*, **110**, 3011-3017.
- Weaver, R.L. and O.I. Lobkis (2004). Diffuse fields in open systems and the emergence of the Green's function, *J. Acoust. Soc. Am.*, **116**, 2731-2734.
- Yang, Y., M.H. Ritzwoller, A. L. Levshin, and N. M. Shapiro (2006). Ambient noise Rayleigh wave tomography across Europe, submitted to GJI.

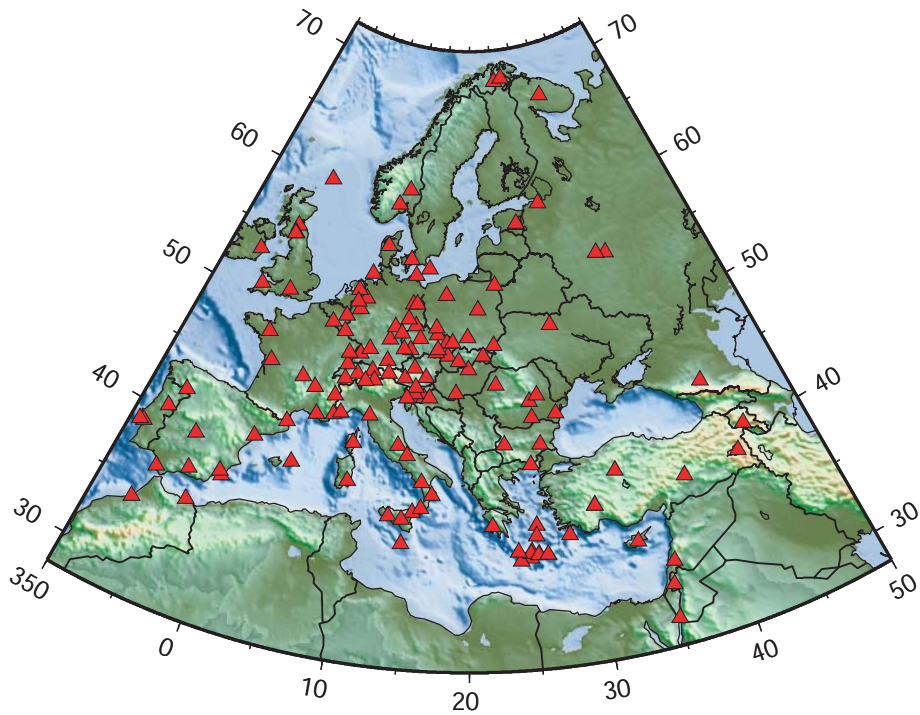


Figure 1. Broad-band seismic stations in Europe used in this study, marked by red triangles.

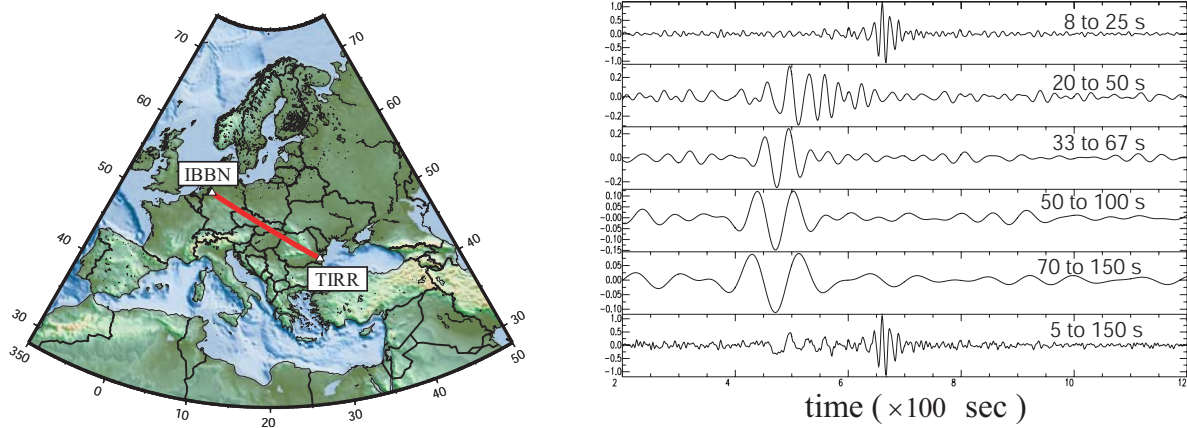


Figure 2. Example of a 12-month broad-band symmetric-component cross-correlation between the station-pair IBBN (Ibbenbueren, Germany) and TIRR (Hungary). The red line shows the great-circle linking the two stations. The broad-band cross-correlation is filtered into five sub-bands. Note the clear normal dispersion of the Rayleigh waves, with the longer periods arriving earlier.

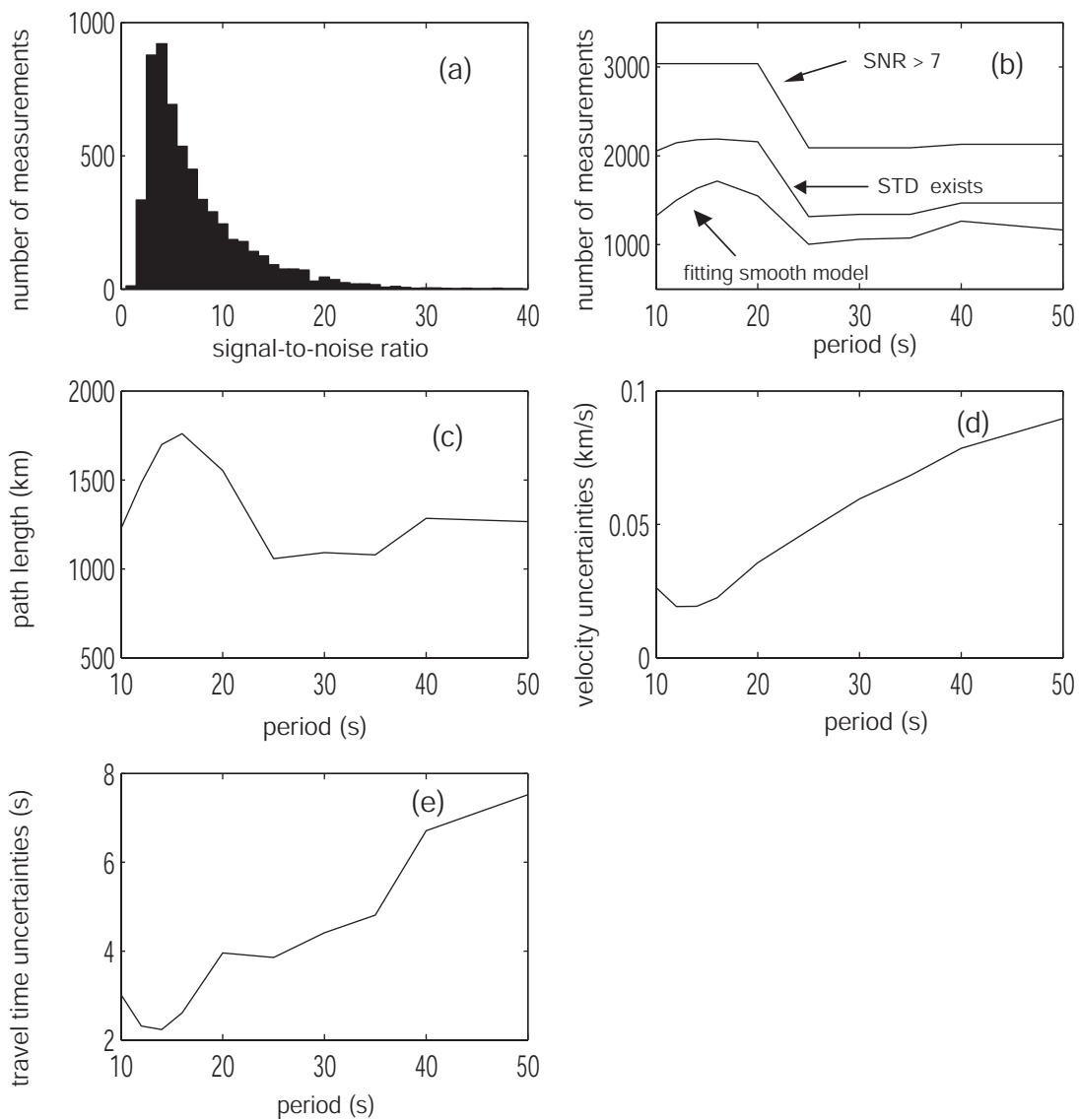


Figure 3. (a) Number of measurements versus signal-to-noise ratio from the 12-month stacked cross-correlations between 20 and 50 sec period. (b) Number of measurements remaining after several steps in data reduction. (c) Average path length of the accepted dispersion measurements. (d) Average group speed uncertainties versus period. (e) Average travel time uncertainties versus period.

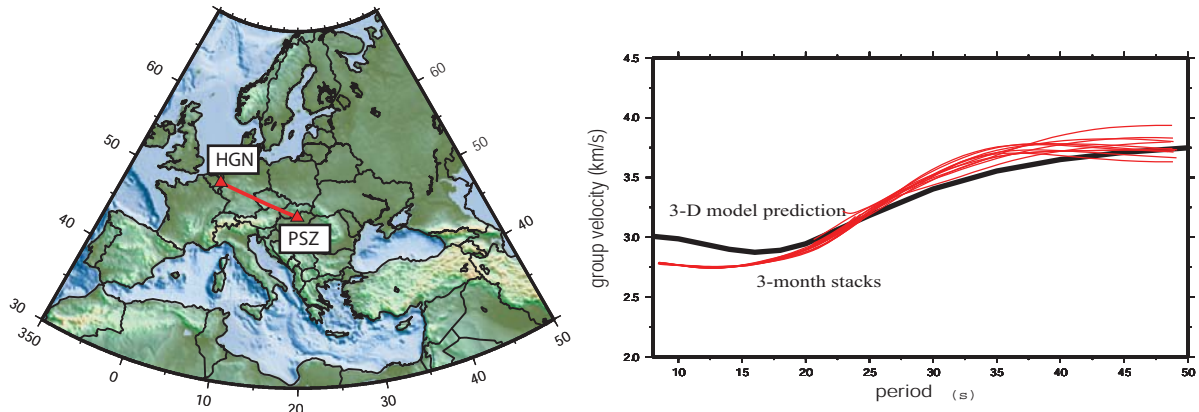


Figure 4. An example of seasonal variability of the dispersion measurements. (left) The path considered is between stations HGN (Heijmans Groeve, Netherlands) and PSZ (Piszkas-teto, Hungary). (right) The red curves are group velocity measurements obtained on twelve 3-month cross-correlations band-pass filtered from 8 to 50 sec period. The black line is the prediction from the global 3-D model (Shapiro and Ritzwoller, 2002).

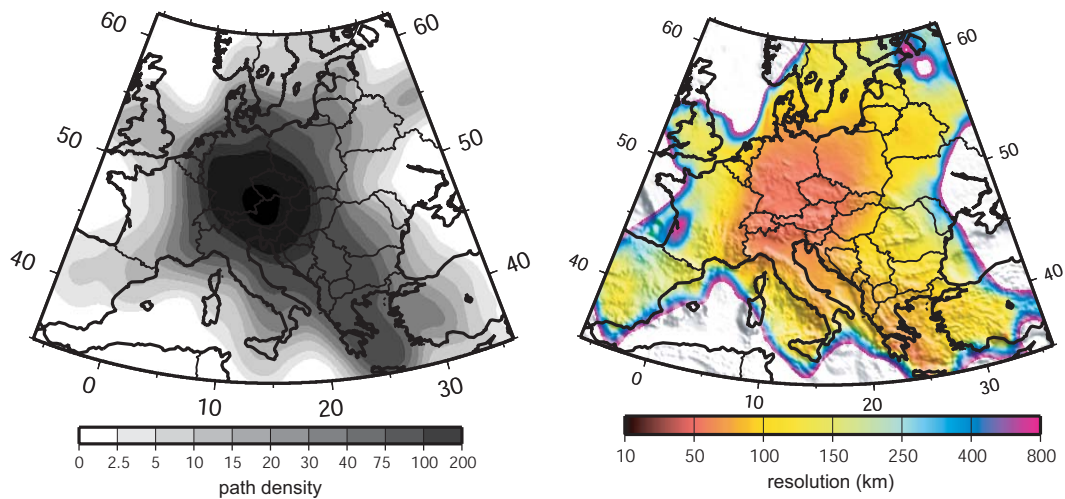


Figure 5. Path density (left column) and resolution estimates (right column) at 16 sec period. Path density is defined as the number of rays intersecting a 111 km x 111 km square cell. Resolution is presented in units of km, and is defined as the standard deviation of a 2-D Gaussian fit to the resolution surface at each model node.

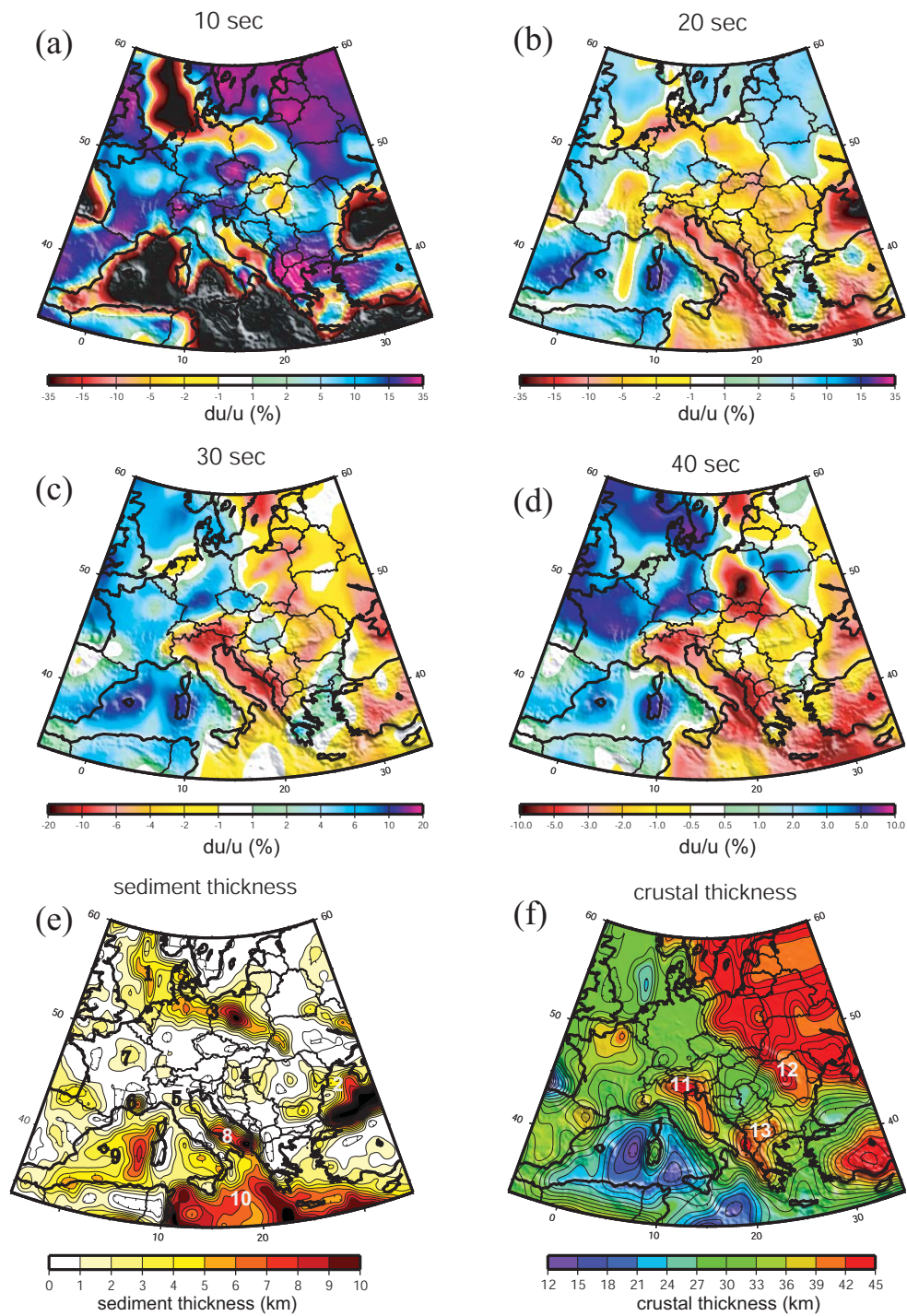


Figure 6. (a-d) Estimated group speed maps at 10, 20, 30, and 40 sec periods. Maps are presented as a perturbation from the average across the map in percent. (e) and (f) Maps of sediment thickness and crustal thickness (Bassin, et al., 2000; Laske and Masters, 1997). The locations of geological units discussed in the text are marked approximately.

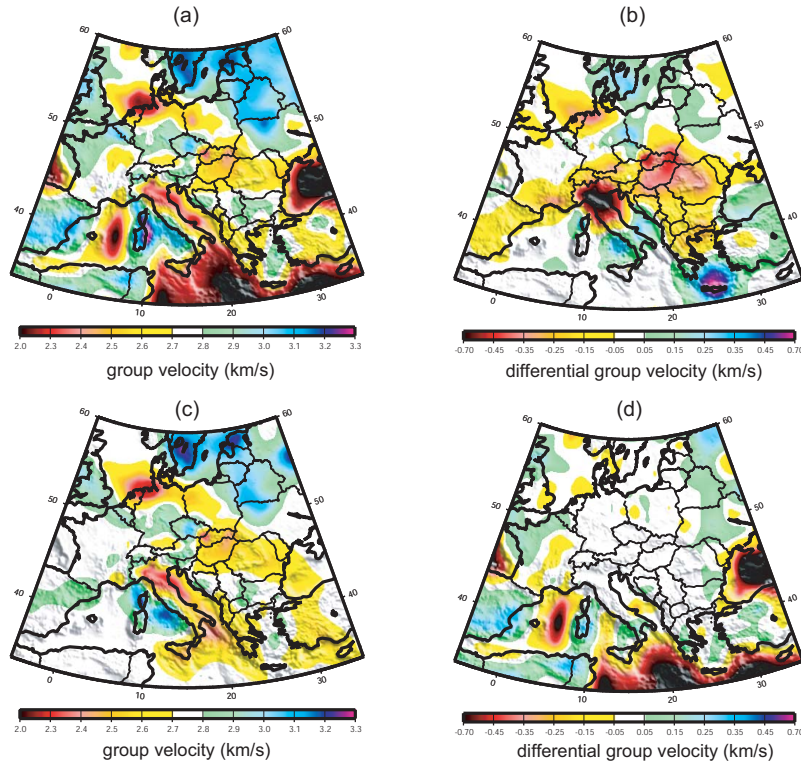


Figure 7. Group speed maps at 16 sec period. (a) Estimated group speed map. A reference map has been used as a starting model in the inversion. (b) Difference between the estimated map in (a) and the reference map. (c) Estimated group speed map determined without a reference map. Comparison should be made with (a). (d) Difference between the two estimated maps in (a) and (c).

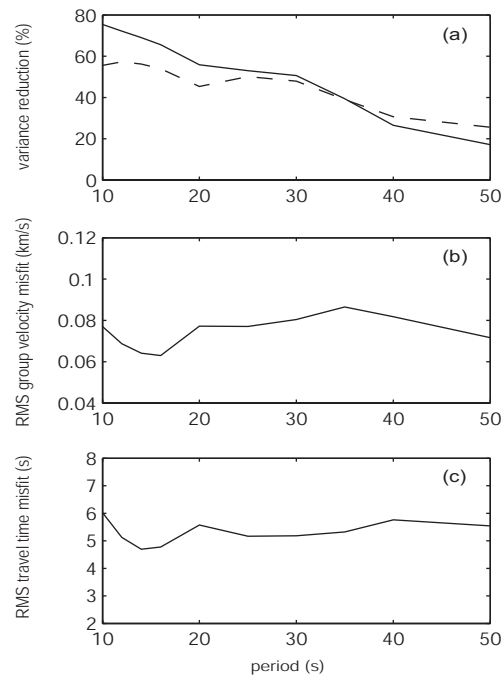


Figure 8. Various misfit statistics for the estimated group speed maps to the observations taken after all stages of data rejection are complete. (Top) Misfit is represented as reduction of variance delivered by (solid line) the estimated maps relative to the predicted group velocity maps from the global 3-D model (Shapiro and Ritzwoller, 2002) and (dashed line) the average velocity across each map. (Middle) RMS group velocity misfit presented versus period. (Bottom) RMS travel time misfit presented versus period.